AGU PUBLICATIONS

Water Resources Research

RESEARCH ARTICLE
10.1002/2014WR015561

Snow depth, density, and SWE estimates derived from GPS reflection data: Validation in the western U. S.

James L. McCreight[1], Eric E. Small[2], and Kristine M. Larson[1]

[1]Department of Aerospace Engineering Sciences, University of Colorado, Boulder, Colorado, USA, [2]Department of Geological Sciences, University of Colorado, Boulder, Colorado, USA

Key Points:
- GPS-based snow depth measurements validated at 18 sites near-peak snow accumulation
- SWE is calculated from snow density modeled on GPS-based depth observations
- Near real-time GPS-based snow depth and SWE are accurate enough for most applications

Correspondence to:
J. L. McCreight,
mccreigh@gmail.com

Citation:
McCreight, J. L., E. E. Small, and K. M. Larson (2014), Snow depth, density, and SWE estimates derived from GPS reflection data: Validation in the western U. S., *Water Resour. Res.*, *50*, 6892–6909, doi:10.1002/2014WR015561.

Received 10 MAR 2014
Accepted 28 JUN 2014
Accepted article online 2 JUL 2014
Published online 25 AUG 2014

Abstract Geodetic-quality GPS systems can be used to measure average snow depth in the ~1000 m^2 area around the GPS antenna, a sensing footprint size intermediate between in situ and satellite observations. SWE can be calculated from density estimates modeled on the GPS-based snow depth time series. We assess the accuracy of GPS-based snow depth, density, and SWE data at 18 GPS sites via comparison to manual observations. The manual validation survey was completed around the time of peak accumulation at each site. Daily snow depth derived from GPS reflection data is very similar to the mean snow depth measured manually in the ~1000 m^2 scale area around each antenna. This comparison spans site-averaged depths from 0 to 150 cm. The GPS depth data exhibit a small negative bias (−6 cm) across this range of snow depths. Errors tend to be smaller at sites with more usable GPS ground tracks. Snow bulk density is modeled using the GPS snow depth time series and model parameters are estimated from nearby SNOTEL sites. Modeled density is within 0.02 g cm^{-3} of the density measured in a single snow pit at the validation sites, for 12 of 18 comparisons. GPS-based depth and modeled density are multiplied to estimate SWE. SWE estimates are very accurate over the range observed at the validation sites, from 0 to 60 cm ($R^2 = 0.97$ and bias = −2 cm). These results show that the near real-time GPS snow products have errors small enough for monitoring water resources in snow-dominated basins.

1. Introduction

Snow is an important environmental variable. It governs energy and water fluxes, influencing both weather and climate [e.g., *Walsh*, 1984; *Cohen and Entekhabi*, 1999]. Snow is also the primary water resource in many areas of the world [*Beniston*, 2003]. Snow depth, snow density, and snow water equivalent (SWE) are fundamental characteristics of seasonal snowpacks. SWE is the liquid depth of melted snow, and thus is critically important for water resources management. SWE is difficult and time consuming to measure [*Sturm et al.*, 2010]. Snow depth is much easier to measure, but it only yields useful information about water storage when combined with measurements or estimates of snow density. Recently, a method has been developed to measure snow depth using networks of geodetic-quality GPS instruments [*Larson et al.*, 2009]. This method has been applied to GPS data collected in the western U.S. (Figure 1), producing snow depth time series that can augment existing snow networks [*Larson and Nievinski*, 2013]. The majority of the GPS sites in this new snow database are part of NSF's Plate Boundary Observatory (PBO), and thus the GPS snow network is referred to as the PBO H_2O project (http://xenon.colorado.edu/portal). A model was also developed to estimate density from these GPS-based snow depth time series [*McCreight and Small*, 2014], allowing for calculations of SWE. In this paper, we assess the accuracy of GPS-based snow depth, density, and SWE data generated at PBO H_2O sites, via comparison to manual observations at 18 sites in the Rocky Mountains.

Snow depth, bulk density, and SWE can be measured on the ground. The simplest snow depth measurement is by manual snow probe [e.g., *Sturm*, 2009]. Similarly, fixed probes have been placed in view of time-lapse cameras to automate the measurement [e.g., *Garvleman et al.*, 2013]. Ultrasonic snow depth sensors also provide automated measurements, including at an increasing number of SNOTEL sites [*Serreze et al.*, 1999]. The spatial footprint of an ultrasonic sensor is ~1 m^2 [*Ryan et al.*, 2008]. Snow depth can be converted to SWE whenever snow bulk density is measured. Bulk density is a labor-intensive measurement that requires digging and sampling a snow pit [e.g., *Dixon and Boon*, 2012]. However, SWE can be directly measured using SWE tubes, such as a federal sampler [e.g., *Farnes et al.*, 1982], as done for snow courses

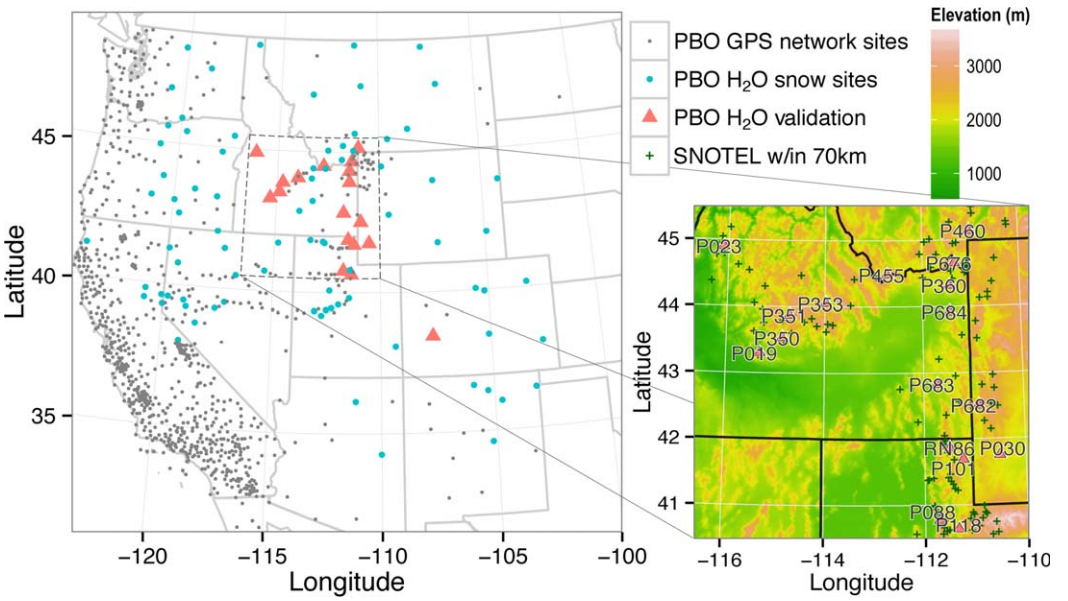

Figure 1. PBO H_2O sites used for validation of the GPS snow products are shown with pink triangles. All other PBO H_2O snow sites are shown in blue. Other PBO GPS locations in the western, continental US are indicated with gray dots. The zoom shows the location of all sites in the study, except for P029 in western Colorado, and the topographic relief of the region. The SNOTEL locations within 70 km of the validations sites, used for density model calibration, are also shown by green crosses in the zoom.

performed by various water districts in the U.S. and Canada [*Cayan*, 1996; *Goodison et al*., 1987]. The sampling footprint of these ground measurements is very small, much less than a square meter. To obtain representative SWE values in the presence of spatial variability, intensive labor is often required (e.g., snow courses). Automated measurements of SWE, found primarily on the SNOTEL network, are performed by pressure sensors with spatial footprints of approximately 3 m^2 [*Johnson et al*., 2007]. Most automated measurements of depth and SWE provide no characterization of local variability in either property. In addition, these measurements do not represent a wide area. Recently, ground-based LiDAR has transformed the ability to measure snow depth over large areas with high accuracy, but these systems remain expensive, are rarely automated, and require bare-earth measurements of terrain elevations [e.g., *Gutmann et al*., 2012].

Satellite and airborne remote sensing techniques have been used to estimate snow covered area (SCA), snow depth, and SWE. Compared to ground-based measurements, satellite estimates generally offer greater continuity in both space and time. Optical data are useful for retrieving SCA at a moderate resolution [*Painter et al*., 2009; *Rittger et al*., 2013]. However, cloud cover poses difficulties. Airborne LiDAR provides high-resolution snow depth measurements, though overflights are typically infrequent if repeated at all [*Harpold et al*., 2014]. Snow depth and SWE are estimated using both passive and active microwave approaches. Microwave retrievals are problematic in many locations. The spatial footprint of passive techniques is very large compared to snow variations. Both microwave approaches remain inaccurate because of uncertainties in snow grain size as well as surface and subsurface snow properties [*Dietz et al*., 2012]. Remote sensing approaches have not provided reliable estimates of snow depth or SWE which are continuous through time.

Larson et al. [2009] first showed that geodetic-quality GPS systems (Figure 2) can be used to measure snow depth. The approach uses active microwave reflectometry in a bistatic geometry (Figure 3), rather than the monostatic geometry typical of satellite remote sensing. This geometry makes the snow depth measurement local to the receiving antenna. Snow depth estimates from multiple GPS ground tracks can be combined, yielding a typical sampling footprint around the antenna of ~1000 m^2. This footprint is much larger than that of in situ snow depth measurements but smaller than satellite microwave measurements. Snow depth estimates from these GPS sites could be used to augment existing snow observation networks, particularly if the GPS-based depth estimates were converted to SWE based on information about snow density.

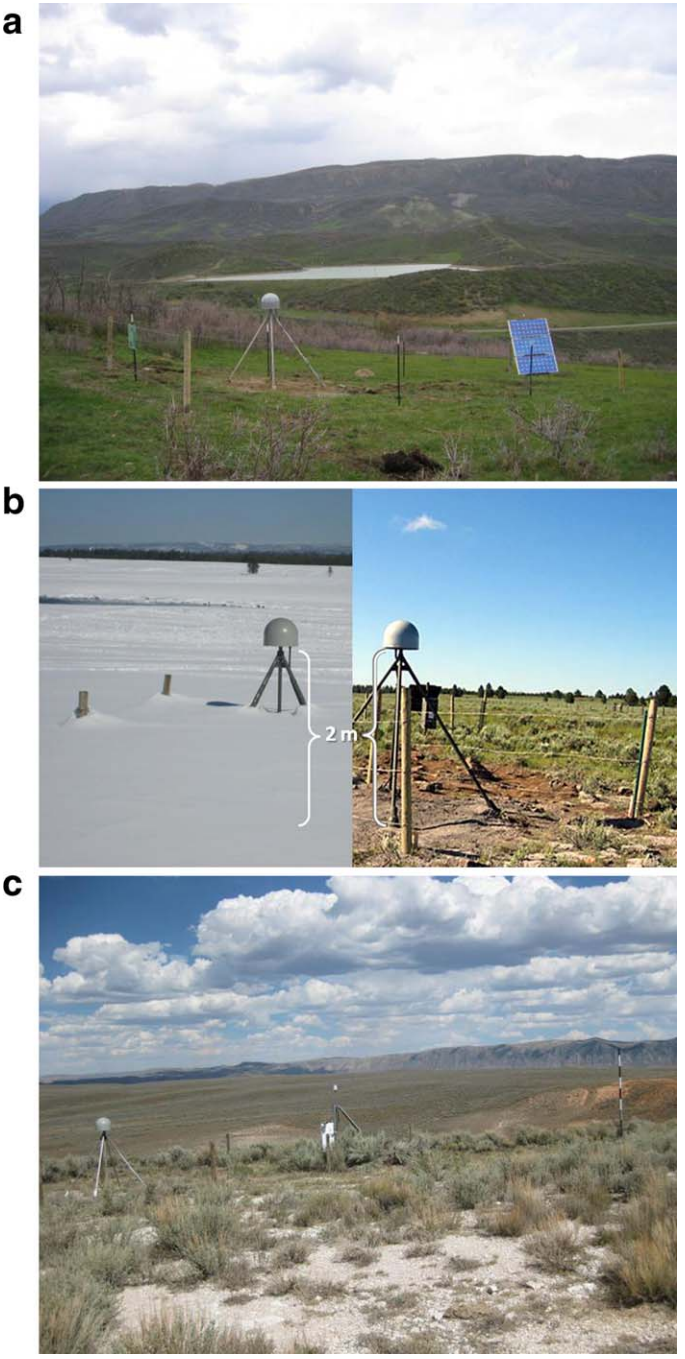

Figure 2. Example of three PBO GPS sites used for validation. (a) P029, Colorado. (b) P360, Idaho, with and without snow. (c) P101, Utah. The black and white pole on the right of image is used for automated photography of snow depth within the GPS footprint.

Previous studies of the accuracy of GPS snow depth measurements were fairly limited in scope. *Larson et al.* [2009] analyzed measurements from two spring snowstorms at an ephemeral snow site near Boulder, Colorado. They showed strong agreement between GPS snow depth estimates, field measurements, and nearby ultrasonic snow depth measurements. *Gutmann et al.* [2012] compared GPS data from an alpine site (Niwot Ridge, Colorado) to terrestrial LiDAR scans and pole measurements. At peak accumulation, they reported an RMSE of 13 cm between LiDAR and GPS. During the melt phase, these errors were slightly smaller. However, the footprints of the LiDAR and GPS systems did not fully coincide and the site had extremely high spatial variability in snow depth. Finally, *Nievinski and Larson* [2014b] compared GPS snow depth retrievals with single snow pole depth observations over multiple years at two sites and manual depth surveys at a third site in a single year. They found a high correlation ($>$0.97) between the GPS and in situ measurements, but stronger conclusions were hampered by the fact that the footprints of the manual and GPS measurements did not coincide.

Here we assess the accuracy of GPS-based snow depth measurements at GPS sites via comparison to extensive field observations. Additionally, we evaluate snow density and SWE estimates that are based on the GPS snow depth time series. Thus, this paper expands upon the previous studies of GPS-based snow depth in three ways. First, we compare GPS snow depth to manual observations at equivalent spatial scales. All of the previous GPS snow depth validation was based on comparisons to depth measured at a point, with the exception of one site used by *Nievinski and Larson* [2014b]. Here the GPS snow depths are compared to manual depth measurements throughout each $\sim$1000 m^2 GPS sensing footprint. Second, we compare manual snow observations and GPS-based snow products at 18 GPS sites in five western U.S., greatly expanding the range of conditions for which the GPS snow products are evaluated. Third, we compare the GPS-based snow density and SWE products to observations. This is the first test of the *McCreight*

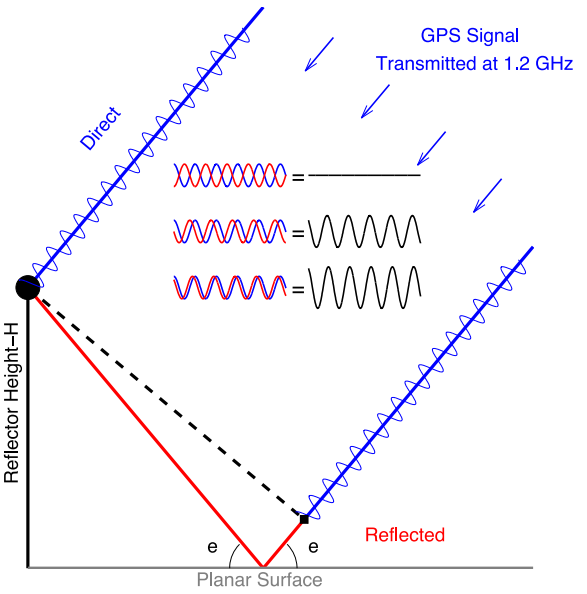

Figure 3. GPS satellites transmit a signal that arrives on the Earth as a plane wave. The ground or snow surface acts as a planar reflector, shown in gray. The antenna is represented by the black circle. The direct signal (blue) travels a shorter distance to the antenna than the reflected signal (blue plus red). The extra path length depends on the elevation angle of the satellite with respect to the horizon, *e*. The GPS carrier signal (wavelength = 24.4 cm) is shown superposed on the direct signal. Depending on the extra path traveled by the reflected signal, the interference between the direct and reflected signals varies (shown for three examples in the center of the figure). This interference (shown in black) is what is measured by the GPS unit in its Signal to Noise Ratio data.

and Small [2014] density model applied to GPS sites. Comparisons between GPS snow products and manual observations focus on the 2 week period near peak snow accumulation, the time most relevant to water management.

The outline of this paper is as follows. The methods section includes a description of: (1) the GPS data and how they are analyzed to estimate snow depth; (2) the manual snow depth and density observations used for comparison to the GPS snow products; and (3) the model used to estimate density and SWE from the GPS-based snow depth time series. In the results, we first compare GPS snow products and manual observations from 18 sites at peak snow accumulation, yielding error estimates for the GPS snow products. Then, season-long observations from three sites are used to put the peak-accumulation analysis in the context of seasonal accumulation and melt. In the discussion, we describe sources of error, evaluate the representativeness of the validation sites, and identify uses for and constraints on existing and future GPS-based snow products.

2. Methods

2.1. GPS Snow Depth Measurement

The GPS snow depth method used by PBO H_2O is described in detail by *Larson and Nievinski* [2013], so here only a brief summary is given. The method uses reflected signals that are transmitted by satellites in the GPS constellation. GPS signals are L-band, with wavelengths of 19 and 24.4 cm on the primary frequencies. The Signal to Noise Ratio (SNR) observable recorded by GPS instruments is sensitive to the interference between the direct signal (used by geophysicists and surveyors) and the reflected signal (Figure 3). As a satellite rises (or sets), the extra path length traveled by the reflected signal changes. The interference pattern will change depending on the elevation angle of the satellite, the signal wavelength, and the height of the GPS antenna above the reflecting surface. The latter quantity, the GPS reflector height, is estimated from the GPS SNR data using a Lomb Scargle Periodogram [*Press et al.*, 1996]. By comparing the reflector heights estimated from snow surfaces to reflector heights estimated from late fall (typically an average for 30 days), when bare soil conditions are prevalent, snow depth can be determined.

A GPS ground track is the path along the surface traced by the specular point of the reflected signal from an individual GPS satellite. The specular point moves toward the antenna as the elevation angle increases. The reflection geometry of ground tracks observed by a GPS antenna depends on its height above the surface. More generally, the satellite geometry depends on the latitude of the GPS receiver and the inclination of the GPS satellites (55°). This results in no satellite tracks between azimuths of ~315–45° in the Rocky Mountain region. In the southern hemisphere, this situation is reversed. Sample reflection (first Fresnel) zones from different satellites are shown for a GPS site in Figure 4. The reflection areas are long ellipses, ~25 m long and ~5 m across for a satellite elevation angle of 10°. The Fresnel zone shown is representative of the average Fresnel zone for the full pass used to derive snow depth, which in this study was for 5–30°. The average sampling footprint given for the GPS method is based on the length of these reflection zones for all visible satellites, which is a region ~1000 m^2 around a GPS antenna that is 2 m above the reflection

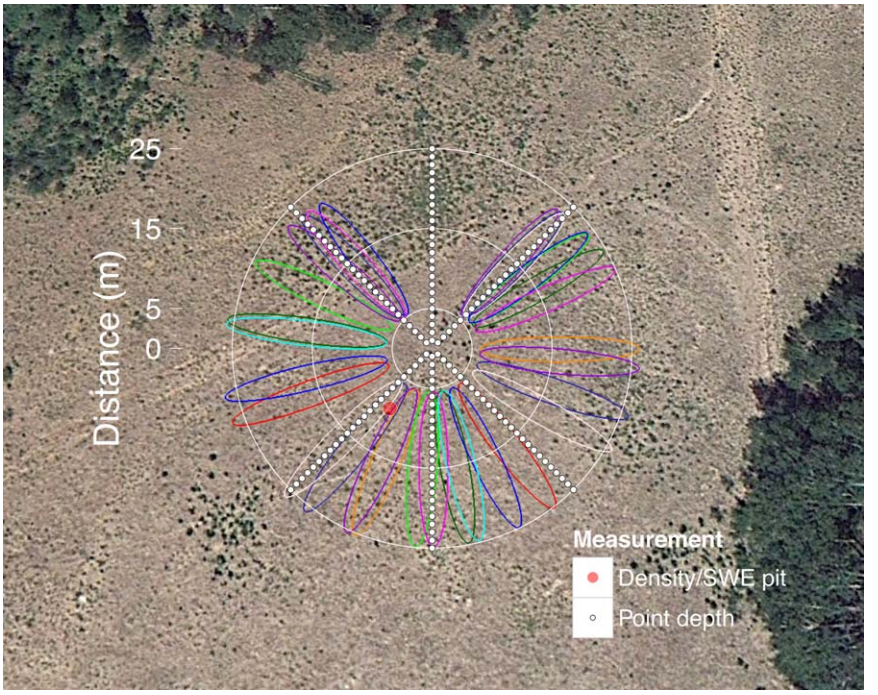

Figure 4. The spatial footprint of the GPS snow depth method is illustrated along with the location of manual observations collected for validation. The GPS footprint is comprised of ground tracks of individual GPS satellites, roughly indicated by different color ellipses. The ellipses actually represent the first Fresnel zones for satellites at 10° elevation angle and for a (snow-free) antenna height of 2 m. The first Fresnel zone is the area of primary surface reflections. It shrinks in size and moves toward the antenna at greater elevation angles and for shorter antenna heights caused by snow accumulation. Only a subset of the GPS ground tracks produces acceptable data to estimate snow depth. The white points illustrate the manual snow depth sampling locations. The red dot indicates the approximate location of snow pits where density and SWE were measured for comparison against modeled values.

surface. One complexity of the GPS snow method is that when a significant amount of snow is on the ground, the Fresnel zones are smaller and closer to the antenna, i.e., the reflection region is smaller. We approximate the radius, r, of the reflection area as a function of snow depth, h_{snow}, using the following equation:

$$r = 21 - 5 * h_{snow} \quad (1)$$

where r and h_{snow} are both in meters. When the snow surface is ~0.5 m or closer to the antenna, snow depth cannot be estimated from the GPS data, and this equation does not apply [*Nievinski and Larson*, 2014a].

The daily snow depth value used in this paper is an average for all snow depths available for individual satellite ground tracks on a given day (UTC time). The number of available ground tracks on the day of the manual snow survey varies from 1 to 12 across the sites (Table 1b). The number of usable ground tracks can vary from site to site as well as over time due to topography, surface roughness, tree cover, and other factors as discussed by *Larson and Nievinski* [2013]. The standard deviation over the snow depths of individual GPS ground tracks which produced measurable estimates of snow depth is combined in quadrature with an uncertainty based on bare soil reflections to provide an error estimate, or standard deviation, on the mean snow depth value. This error is not a true measurement error because it encompasses variability in snow depth around the antenna. We know the GPS method fails if the snow level becomes too close to the antenna. Simulations show that the snow surface should be ~50 cm (two wavelengths) from the antenna [*Nievinski and Larson*, 2014a]. Readers seeking greater detail on the GPS measurement technique are directed to *Larson and Nievinski* [2013].

The PBO H_2O group currently estimates snow depth for 155 sites. Twenty-five sites are in Alaska; the remaining sites are primarily located in the western U.S.: Idaho, Montana, Wyoming, Oregon, Washington,

Table 1a. General Site Information

Site:	P019	P023	P029	P030	P088	P101	P118	P350	P351	P353	P360	P455	P460	P676	P682	P683	P684	RN86
Longitude (°W)	115.3	116.1	107.6	110.5	111.7	111.2	111.3	114.9	114.7	114.0	111.5	112.7	111.0	111.3	110.9	111.7	111.5	111.5
Latitude	43.3	44.9	38.4	41.7	40.8	41.7	40.6	43.5	43.9	44.1	44.3	44.5	45.1	44.7	42.5	42.8	43.9	41.9
Elevation (m)	1683	1522	2456	2150	1921	2016	2083	2388	2693	2041	1858	2594	2198	2190	2324	2066	1694	2591
State	ID	ID	CO	WY	UT	UT	UT	ID	ID	ID	ID	ID	MT	ID	WY	ID	ID	UT
Landcover.Type[a]	G	G	S	G	S	OS	G	G	WS	G	G	WS	WS	G	EN	OS	CL	EN
Antenna Height (m)	1.85	2.11	1.86	1.84	1.93	1.90	1.96	1.91	1.81	1.28	2.15	1.30	1.74	1.46	1.76	1.68	1.93	3.12
Average Maximum Snow Depth (cm)	56	74	77	47	31	70	37	144	126	2	87	81	19	80	84	45	37	184

Table 1b. Near-Peak Accumulation Validation Snow Data[b]

Site:		P019	P023[c]	P029[c]	P029	P030	P088	P101	P118	P350	P351	P353	P360	P455	P460	P676	P682	P683	P684	RN86	RN86
Year		2012	2012	2012	2013	2012	2012	2012	2012	2012	2012	2012	2012	2012	2012	2012	2012	2012	2012	2012	2013
Day of year		75	74	67	85	69	68	69	68	93	93	76	71	94	73	72	69	70	71	55	114
# of GPS Tracks		5	3, 2	4	5	8	4	9	9	3	4	7	12	5	4	3	1	6	10	6	7
Depth (cm)	GPS	39.9	71.2	67.9	67.2	0.0	10.5	27.3	29.5	138.8	131.4	0.0	75.0	66.7	9.8	41.4	41.1	47.0	0.0	143.9	138.0
	Transects	34.5	72.7	73.6	73.4	0.0	16.7	25.2	37.9	146.4	154.7	0.0	87.8	64.2	14.1	72.7	59.5	62.0	0.0	140.1	141.8
Stdev Depth (cm)	GPS	6.4	10.7	5.2	5.3	4.3	3.3	5.3	4.3	4.8	4.3	3.8	4.0	3.3	5.6	2.7	5.0	7.1	3.0	13.2	5.9
	Transects	1.3	1.0	6.8	5.2	0.0	5.5	8.7	7.9	5.3	12.9	0.0	5.8	32.6	5.2	27.4	7.4	5.9	0.0	3.2	1.5
	Points	5.0	4.7	10.9	10.4	0.0	12.1	14.9	9.5	7.1	20.9	0.0	9.0	33.5	12.1	31.4	18.9	8.7	0.0	4.6	4.7
Density ($g*cm^{-3}$)	GPS	0.33	0.33	0.26	0.30		0.27		0.25	0.35	0.36		0.27	0.29	0.26	0.27	0.29	0.27		0.28	0.42
	Pit	0.44	0.28	0.28	0.30		0.24		0.29	0.37	0.34		0.27	0.33	0.24	0.27	0.27	0.28		0.30	0.39
SWE (cm)	GPS	13.2	23.8	17.7	20.4	0.0	2.8		7.4	49.0	46.7	0.0	20.2	19.3	2.5	11.3	12.1	12.7	0.0	39.6	58.5
	Pit	15.0	20.3	20.9	22.2	0.0	4.0		10.9	54.4	52.6	0.0	24.0	21.1	3.4	19.4	16.2	17.5	0.0	42.6	55.3

[a]Grassland, S=Savannas, OS=Open Shrubland, WS=Woody_Savanna, EN=Evergreen Needleleaf, C=Crop Lands (Determined from local photographs and MODIS landcover classifications.)

[b]GPS snow depth is the mean calculated from all usable tracks. Standard deviation of in situ snow depth is calculated in two ways: (1) standard deviation of the transect-mean snow depths; and (2) the standard deviation over all manual point measurements. Density is not reported for sites with no snow.

[c]GPS values are interpolated from observations on adjacent days as no observations were available on the day of manual measurement. Number of GPS tracks is shown for both days.

Colorado, Utah, California, and Nevada (Figure 1). With few exceptions, these sites were installed to measure position, either by geophysicists (PBO) or to support surveyors. This means that the antennas were placed to ensure visibility to the direct GPS signals so that positioning precision could be optimized. This also means that no GPS sites are located below trees, i.e., near forested regions. The location of GPS sites installed by geophysicists for the Plate Boundary Observatory was dictated by geologic features, and thus is often found far from urban areas. GPS sites installed by surveyors are installed in both urban and rural areas.

2.2. In Situ Observations

We selected 18 PBO H_2O snow sites in Colorado, Utah, Wyoming, Montana, and Idaho to validate (Figure 1 and Table 1) during the manual survey. These sites were chosen based on three criteria. First, the sites were located along a relatively direct route, allowing the field crew to visit one or two sites per sampling day. Second, the validation sites needed to be representative of the entire population of PBO H_2O snow sites in terms of the number of usable ground tracks. Third, we needed access to the site for sampling. Some GPS sites in the network are relatively inaccessible during the winter, requiring more than a day of backcountry travel from the nearest road. Other sites were excluded due to land-owner constraints.

In this study, we compare the mean snow depth based on all available GPS ground tracks to the mean snow depth measured throughout the maximum-possible 1000 m^2 sampling footprint, which is a quantity of interest for water resources applications. For this reason, the following sampling procedures were followed at each site. Snow depth was measured every meter along six transects, each extending from the antenna to a distance of 25 m. This distance was selected based on the sensing footprint for a standard height (2 m) GPS antenna (Figure 4). Snow depth was measured via snow probe and depth was recorded to the nearest centimeter. In the absence of snow at any sampling location, a zero depth was recorded. Transect azimuths were the same at all sites (Figure 4). Azimuths were chosen to evaluate if GPS measures a representative average snow depth over the 1000 m^2 around the antenna. Therefore, three transects were located to the north of the antenna and three to the south, even though most GPS tracks are to the south of the antenna (in the northern hemisphere). At most sites, this protocol yielded 150 measurements of snow depth. At several sites, topographic constraints (e.g., a cliff) or vegetation precluded measurements of depth at some planned sampling locations, yielding fewer total measurements.

Density was measured at a single snow pit in the GPS footprint. Pits were located ~10 m to the southeast or southwest of each antenna, with the exact location depending upon site access and location of infrastructure (e.g., solar panels, cattle fences, etc.). A 1000 mL snow cutter was inserted into the face of the pit at 10 cm intervals from the snow surface to the ground. The mass of snow was measured and density calculated from the known volume excavated [e.g., *Elder et al*., 1991]. Density was measured after snow depth. This allowed us to dig the snow pits in locations with snow depth typical of each site. Modeled snow densities are compared to the single observed pit value at each site.

In section 3, we assess if GPS-based SWE represents the average SWE in the GPS footprint. We calculate observed, areal-average SWE as the product of the single density measurement and the average snow depth found by probing the footprint. We acknowledge that this calculation is only an approximation because of potential spatial variability in density and its nonlinear dependence on snow depth, particularly for snow depths above 80 cm [*Pomeroy and Gray*, 1995; *Sturm et al*., 2010]. However, this approximation is reasonable and often made in practice due to the difficulty of measuring snow density spatially and because density varies much less than snow depth over the same area [*Dickinson and Whitely*, 1972; *Stephun and Dyck*, 1974; *Marchand and Killingtveit*, 2004; *Elder et al*., 1991]. The only location which challenges this assumption in our study is P455, which exhibited extreme spatial variability in snow depth.

Seventeen of the sites were visited once during February or March of 2012, within approximately 1 week of observed peak accumulation at each site. One site of these sites (P029) was revisited in 2013, again near the time of peak accumulation. The RN86 site was visited six times in both the 2012 and 2013 water years. Density and SWE were measured during five of the six visits in each year. Our main validation data set consists of 20 total observations at 18 distinct locations made around the time of peak accumulation (Figure 1 and Table 1). We include all 17 observations from 2012, the observation at P029 in 2013, and the observations at RN86 in each year with the largest snow depth. Only 16 of these depth observations have associated density observations as three locations had no snow and it was not possible to measure density at one location. Though manual observations were collected at p351, no GPS data were available within a week of these. From the earlier GPS observations, it could be inferred that snow had encroached on the antenna and the manual observation confirmed this. Therefore, the data from P351 (Table 1) are not included in the analysis.

After validation of estimates at peak accumulation, additional time series data from three sites are analyzed to examine the suitability of GPS for measuring seasonal snow accumulation and melt. Time-lapse photography was used at two sites (P360 and P101) to provide depth estimates at single points within their GPS footprints. A fixed snow pole was photographed three times per day, and these observations were averaged to a single daily depth value. The 12 manual surveys at RN86 are also used to assess the seasonal progression of accumulation and melt.

2.3. Density Model and SWE

The GPS method provides estimates of snow depth, but information about SWE is needed for many applications. Given snow depth, snow bulk density can be used to calculate SWE. Snow bulk density varies within a narrow range and can be estimated based on snow depth and other predictors [*Jonas et al*., 2009; *Sturm et al*., 2010]. In contrast, snow depth varies greatly. Snow depth is therefore the more important factor in

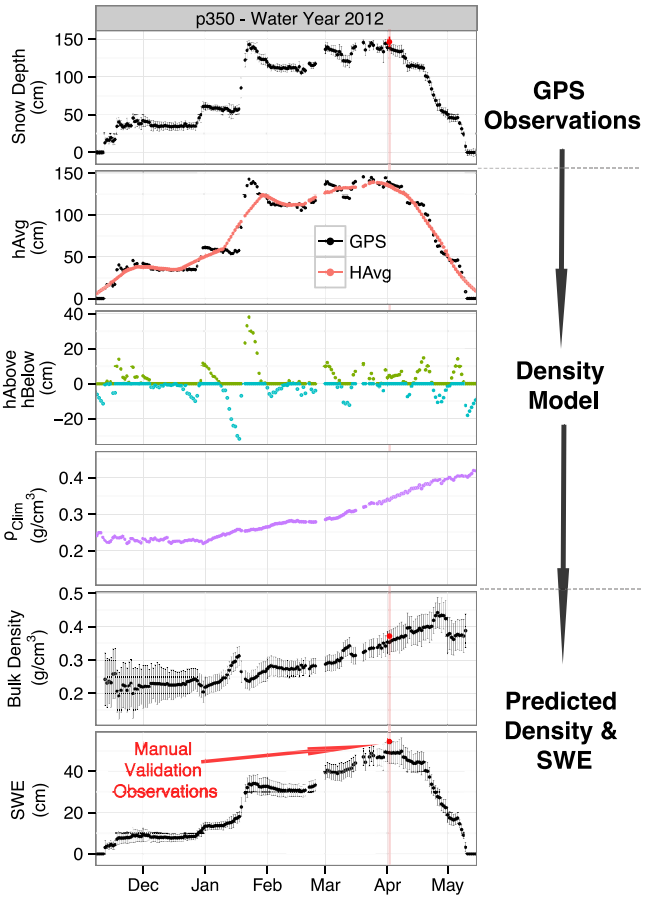

Figure 5. Example density and SWE calculation for site P350. All error bars represent ±1 standard deviation. Plot 1: GPS snow depth observations, the primary input to the density model. Plots 2–4: model predictors; hAvg is computed using the GPS snow depth and a centered, 21 day window; Anomalies (hAbove and hBelow) of observed snow depth relative to hAvg; and daily climatology of fit, ρClim. Plot 5: modeled bulk density. Plot 6: estimated SWE. The red points overlaying the GPS estimates indicate the manual, validation measurements of depth, density, and SWE. The vertical red bar highlights the day of validation near-peak snow accumulation.

determining SWE. For this reason, errors in modeled density have a limited effect on SWE errors when depth is observed. For example, the model of *McCreight and Small* [2014] explained only 56% of the observed variance in density throughout the snow season and 71% of the variance near peak accumulation, which was greater than the other models considered in their study. Though the density model was not very accurate, 96% of the observed SWE variance was explained when modeled densities were multiplied by known snow depths, both for the full snow season and near-peak accumulation. This demonstrates that even if the density model is imperfect, useful SWE estimates can be obtained if GPS-measured snow depth is accurate.

The *McCreight and Small* [2014] bulk density model, illustrated in Figure 5, was developed to transform daily snow depth observations to SWE. The model recognizes that snow depth and bulk density are negatively correlated at short (10 days) time scales while positively correlated at longer (90 days) time scales. Previous models focused on longer time scales while neglecting how daily snow accumulation and ablation tend to decrease and increase bulk density, respectively. *McCreight and Small* [2014] modeled density over both short and long time scales by separating observed snow depth time series into three components, used as predictors of density in a linear regression model. The long time scale variability is modeled using a running average snow depth, *hAvg*, computed on a window of 21 days (plot 2 of Figure 5). Short time scale variability is modeled by anomalies from this average. These anomalies are separated into two different predictors by sign, *hAbove* and *hBelow* (plot 3 of Figure 5). A fourth predictor is a daily climatology of fit, ρ_{Clim} (plot 4 of Figure 5).

The regression model is given by the following equation:

$$\rho(h, month, neighbors) = a * hAvg + b * hAbove + c * hBelow + d * \rho_{clim} + e \quad (2)$$

Application of this model to a GPS site, where density is not observed, requires solving the model parameters using observations of the relationship between depth and density. We solve these parameters for each PBO H_2O site separately on a monthly basis, using collocated depth and density data from SNOTEL sites within 70 km of the GPS site. There are between 3 and 34 SNOTEL sites within 70 km of each PBO H_2O site. At each site, observed snow depth, *h*, from each SNOTEL is split into the three new predictors described above. The ρ_{Clim} predictor for each GPS site is calculated as the average observed density on each day of the year over the set of neighboring SNOTEL sites. Ordinary least squares estimation is used to solve for the model parameters against the observed densities. At each GPS site, density is then modeled using the GPS-

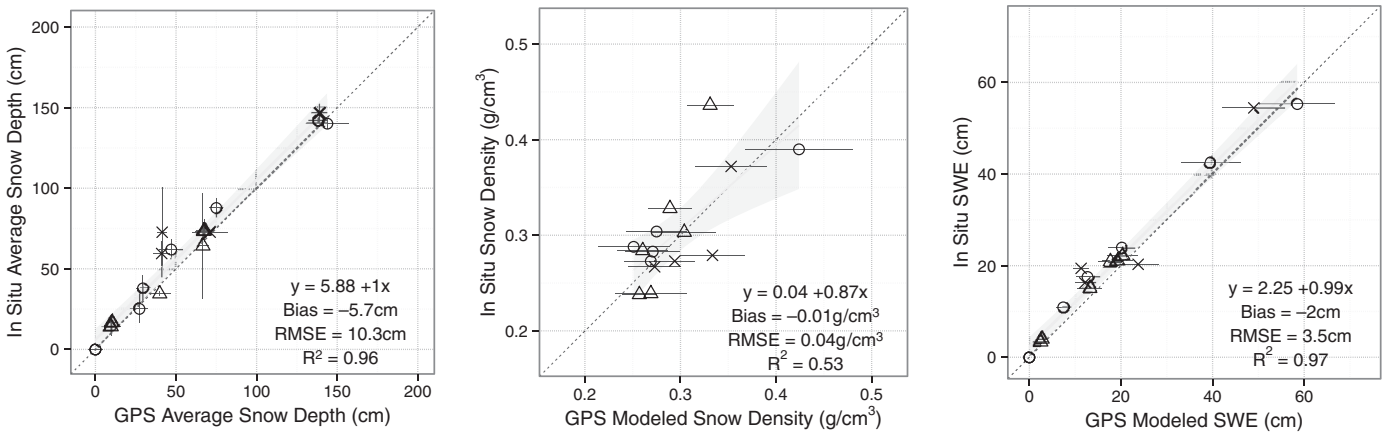

Figure 6. GPS versus manual snow depth, density, and SWE at 18 PBO H_2O sites near peak accumulation. The individual values are presented in Table 1. Symbols indicate the number of ground tracks used to estimate depth: cross is 1–3, circle is 4–5, and triangle is 6–12. Error bars represent 1 standard deviation. The 1-1 line is dashed. The regression relationship with standard error of fit is shown by a solid gray line and a shaded area. Coefficients of fit and statistics (including snow-free observations of depth and SWE) are shown in the plots.

observed snow depths, the five parameters estimated for that site, and the density climatology. Finally, SWE is calculated as the product of modeled density and observed depth.

Uncertainty in modeled density (e.g., error bars in Figure 5, plot 5) at a GPS site is estimated by treating each SNOTEL site used for training as if it were a GPS site and characterizing the set of density errors resulting from this leave-one-out cross validation. Following the model fitting procedure above, each SNOTEL site is withheld in turn from the parameter fitting process. Its observed densities are then estimated from its observed snow depths using the parameters and climatology derived from the remaining SNOTEL sites. This yields a set of density errors (modeled-observed) that result from model structural errors and from parameter transfer to a location where density is not observed. For each day of year, the standard deviation of these errors describes the uncertainty in the model estimate at the GPS site. For example, there are 34 SNOTEL sites within 70 km of P118. At each of these SNOTEL sites, the time series of observed densities is estimated using parameters and the climatology based on the remaining 33 SNOTEL sites while using its own observed snow depths for the predictor variables. The density errors over all water years at all 34 SNOTEL sites are then collected by day of year. The standard deviation of these errors on each day of year describes the uncertainty in density estimation for the GPS site on that day.

Uncertainty described by this cross-validation process includes error resulting from parameter transfer between SNOTEL sites. Parameter transfer between SNOTEL sites contributed 2.6 cm to SWE RMSE scores at a site [*McCreight and Small*, 2014]. Physiographic differences between SNOTEL and GPS sites are greater than between SNOTEL sites, which could mean larger errors from parameter transfer. GPS sites tend to be at lower elevations than the SNOTEL sites within 70 km that are used for estimating parameters. In addition, GPS sites are located in large clearings or nonforested areas, whereas SNOTEL are mostly located amidst forests. This leads to differences in exposure to wind and radiation (both long wave and solar). As a result, uncertainty in density estimates may be underestimated for PBO H_2O sites. Our calculated uncertainty in SWE combines the uncertainties in modeled density and in GPS-observed snow depth. SWE standard deviations are calculated for each day of year as the vector sum of the (assumed) independent depth and density standard deviations.

Interpreting the spatial scale represented by modeled density and SWE is not straightforward. Though we validate against point density measurements and estimates of areal-average SWE, we can claim only that these modeled quantities represent the best possible estimates based on available data. Likewise, error estimates for modeled density and SWE represent a best attempt at quantifying their uncertainty.

3. Results

3.1. Peak SWE Observations

Snow depth and SWE were relatively low in many parts of the western U.S. during the 2012 snow year. Depending on location, depth, and SWE in 2012 were as much as 50% below normal. Three sites (P030,

Table 2. GPS Snow Depth and SWE Statistics Calculated in Four Ways[a]

	Including Snow-Free Obs.	GPS Footprint Depends on Snow Depth	Bias (cm)	RMSE (cm)	R^2
Snow Depth (cm)			-6.7	11.3	0.95
	✓		-5.7	10.3	0.96
		✓	-6.2	10.3	0.96
	✓	✓	-5.2	9.5	0.97
SWE (cm)			-2.5	3.8	0.97
	✓		-2.0	3.5	0.97
		✓	-2.3	3.6	0.97
	✓	✓	-1.9	3.3	0.97

[a]The three sites with no observed snow on the day of the manual survey are either included (checked) or excluded. Manual observations from either the smaller, snow-depth-dependent footprint (checked) or the larger, snow-free GPS footprint are also compared.

P353, P684) had no snow at the time of the 2012 survey (Table 1). In most years, maximum snow depth at P030 and P684 is more than 0.5 m and their average maximum snow depth over all year of GPS observation is greater than 0.35 m (Table 1a). Snow is ephemeral at P353 and rarely exceeds 10 cm (Table 1a). We include data from these three sites in our comparison.

3.1.1. Snow Depth

At each site, the mean GPS snow depth closely matches the mean depth measured in situ (Figure 6, top). This indicates that site-average GPS depth estimates provide a reliable measure of snow depth within a 25 m radius of the antenna, or at the ~1000 m^2 scale. The depth comparison spans a broad range, from no snow to 150 cm, with GPS explaining 96% ($=R^2$) of the observed variance. There is a small negative bias (−5.7 cm) that is consistent across the range of snow depth. The RMSE between GPS and in situ depth is 10.3 cm. When the bias is removed, RMSE decreases to 8.7 cm. As discussed above, three sites had no snow or very little snow during the 2012 survey. At these sites, the GPS depth measurements match the observed, zero snow depths. Summary statistics are effectively the same when observations from these snow-free sites are excluded from the comparison (Table 2).

The number of GPS ground tracks that yield usable data varies between sites and through time. On the days that in situ data were collected, the number of ground tracks used at each site varies from 1 (P682) to 12 (P360; Table 1b). The symbols used in Figure 6 indicate the number of GPS tracks used to calculate the GPS mean snow depth on the day of the manual observation. The largest differences between GPS and mean in situ depth are at P676 and P682, where only three and one tracks (respectively) were used to calculate the site-average GPS depth. Site-average GPS depths were based on less than four tracks at only two other sites. When data from these four sites are excluded, the bias is reduced to only −3.2 cm and RMSE to 6.6 cm (unbiased RMSE to 5.8 cm). This result is expected: when more ground tracks are used to calculate the site average, the correspondence with average snow depth measured in situ should be closer. This is especially true at sites with significant snow depth variability over the GPS footprint.

Figure 6, top, compares the mean GPS snow depth at each site with the corresponding mean of all in situ observations within 25 m of the antenna. However, the length of each GPS ground track on a given day depends on the antenna height above the reflecting surface: as snow depth increases, the reflection area decreases (section 2.1). We recalculate the statistics to compare the mean GPS depth with the mean of the in situ observations falling within the depth-dependent ground track radius (equation (1)). The mean in situ snow depth is used to estimate the ground track length at each GPS antenna. For example, at sites with ~150 cm of snow, the average in situ observation only includes data within ~10 m of the antenna. Table 2 summarizes the validation statistics considering the fixed, snow-free footprint (~20 m radius) and the footprint that varies as a function of snow depth. The statistics are nearly identical regardless of which subset of in situ data is used. Statistics based on depth-dependent track length excluding the three snow-free observations are also very similar.

3.1.2. Snow Depth Variability and GPS Accuracy

We observed a wide range of snow depth variability within the sensing zone at the validation sites. Table 1b shows both (1) the standard deviation of the 150 manual points at each site, varying from 4.6 to 33.5 cm; and

(2) the standard deviation of the six manual transect mean values at each site, varying from 1.0 to 32.6 cm. The vertical error bars in Figure 6 (top) represent the latter value. These can be more directly compared to variability of depth estimates calculated over individual GPS ground tracks. Sites P676, P682, and P455 had the greatest snow depth variability (as did P351, which was not included in the validation comparison because snow encroached on the antenna). Their manual point measurements ranged over 91 cm and their standard deviations ranged from 19 to 34 cm (Table 1b). The greatest variability between manual transects was observed at P676 and P455. Among these three sites, P455 had the greatest snow depth variability. Roughly 20% of the sampled area had no snow, whereas snow depth exceeded 1 m along a 6 m portion of the transect to the northwest of the antenna. The remainder of the sites showed much less spatial variability (Table 1b).

There is a potential for large differences between the GPS depth and the mean in situ snow depth at sites where there are few usable GPS ground tracks and snow depth is variable. The usable GPS ground tracks may be located in parts of the GPS footprint that have snow depth well above or below the mean. The two greatest GPS snow depth errors occur at sites with high variability and few usable ground tracks. Site P676 has the largest absolute GPS snow depth error. At this site, there were only three usable ground tracks, which were clustered within 50° of azimuth. As a result, the GPS depth estimate represents only ~15% of the 1000 m^2 area around the antenna. Comparison of the manual transect that is closest to the three usable GPS tracks yields a bias of −10 cm, instead of −31.3 cm. Significant snow depth variability was also observed at site P682 where only one GPS track was available on the day of observation. This site had the second largest (−18 cm) error. P455 had the smallest absolute error (2.5 cm) of the sites with greatest spatial variability, probably because the five usable GPS tracks were distributed across the GPS footprint.

We now evaluate if the intertrack variability at a site provides an accurate measure of snow depth spatial variability within the GPS footprint. The following two measures of variability are compared: (1) the standard deviation of the depths estimated from the individual GPS tracks and (2) the standard deviation of the mean snow depths of the (six) manual transects at each site. Analysis indicated no meaningful relationship ($R^2 = 0.12$) between these measures of variability. Similarly, there is no meaningful relationship between intertrack variability and standard deviation of all manual points at a site.

3.1.3. Bulk Density

Modeled and observed snow bulk densities are compared in the middle plot of Figure 6. Each modeled value is based on (1) the time series of snow depth estimated from GPS data at that site and (2) model parameters (equation (1)) and climatology of fit determined from neighboring SNOTEL sites. As shown in the P350 example (Figure 5), density is predicted for all days on which snow depth estimates exist. Only the modeled density from the day field data was collected is used for validation. Modeled and observed densities vary from 0.25 to 0.45 g cm^{-3} across the 16 density measurements, with the highest density values corresponding to the deepest snow. Model bias is effectively zero (<0.01 g cm^{-3}) and RMSE is 0.04 g cm^{-3}. This is equal to the RMSE for the model applied to SNOTEL sites, using data around the time of peak SWE [*McCreight and Small*, 2014]. However the R^2 value (0.53) is lower than found (0.71) when the model is applied to SNOTEL sites.

The two largest density errors were −0.11 g cm^{-3} at P019, though GPS-measured mean snow depth was relatively accurate, and 0.05 g cm^{-3} at P023. The density RMSE is dominated by these two errors and excluding them halves the density RMSE to 0.02 g cm^{-3}. In the discussion, we consider these large modeled density errors in more detail. Density errors of the remaining 14 observations are small and arise due to several factors, including measurement error, variability of density at a site, and parameter transfer.

3.1.4. SWE

The bottom plot of Figure 6 compares in situ and GPS-based SWE values. The GPS SWE data accurately ($R^2 = 0.97$) portray the observed variations across the 18 sites, from 0 to 60 cm SWE. Bias and RMSE in SWE are essentially those of snow depth scaled by the density. Thus, the roughly −6 cm bias in depth becomes a −2 cm bias for SWE, and the depth RMSE of 10.3 cm becomes 3.5 cm. Excluding sites with less than four tracks available for calculating depth decreases these error statistics by about 30%. These results show that the GPS reflections method yields SWE data at GPS sites with errors that are small enough for most applications.

3.2. Time Series Observations

In this section, we compare time series from GPS and in situ observations at three sites. This comparison is intended to supplement the peak-accumulation validation data described in section 3.1. RN86 was the only

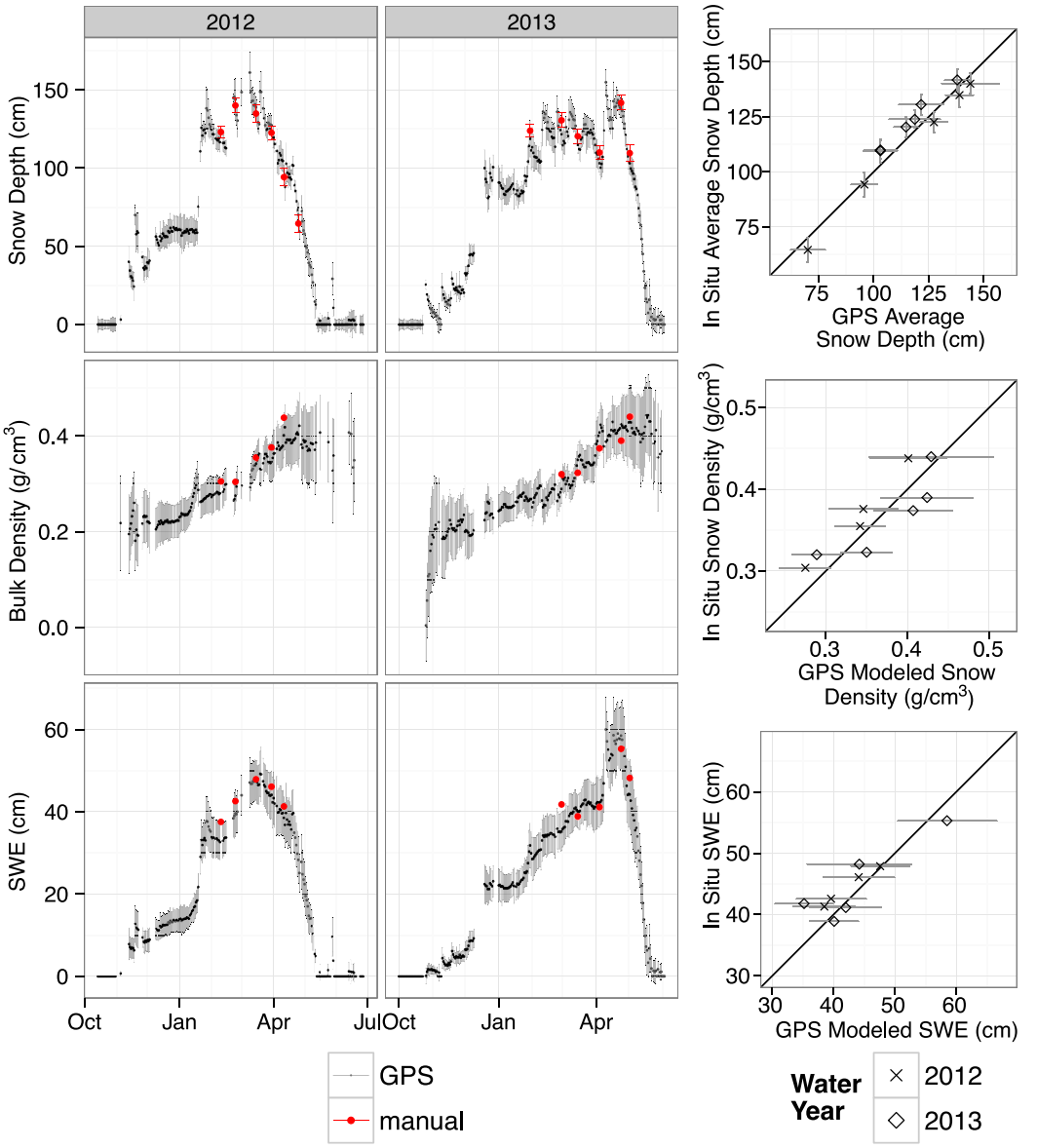

Figure 7. (left and middle columns) Time series of GPS snow depth measurements, modeled density, and SWE estimates at the RN86 site and manual measurement in red. Uncertainty is represented by ±one standard deviation error bars. Error bars on the manual measurements represent the standard deviations over all snow depth points surveyed (not transect-mean snow depth). (right column) A scatterplot of all corresponding GPS and manual observations at RN86 for each variable.

site where it was feasible to complete manual depth and density observations multiple times per season. In 2012 and 2013, manual observations were completed at RN86 approximately every 3 weeks between January and May. Only the observations with the largest depth measurements from each year were included in the peak-accumulation validation analysis above. Figure 7 (top row) shows the time series of GPS and manual snow depth observations from RN86. GPS-derived snow depth closely matches observed depth throughout the season, not only at peak accumulation. Over the 2 years, the GPS snow depth bias is −2 cm and RMSE is 5.5 cm. The observed and modeled density time series are compared in the middle row of Figure 7. As is the case for depth, modeled density is very similar to observed. Bias is −0.01 g cm^{-3} and RMSE is 0.03 g cm^{-3}.

The bottom row of Figure 7 compares SWE time series. Over the 10 observations, SWE bias is −1.5 cm and RMSE is 3.2 cm. GPS-based SWE underestimated the first two manual observations in 2012 because both the GPS snow depth and the GPS-modeled density were underestimated. By mid-March 2012, GPS SWE

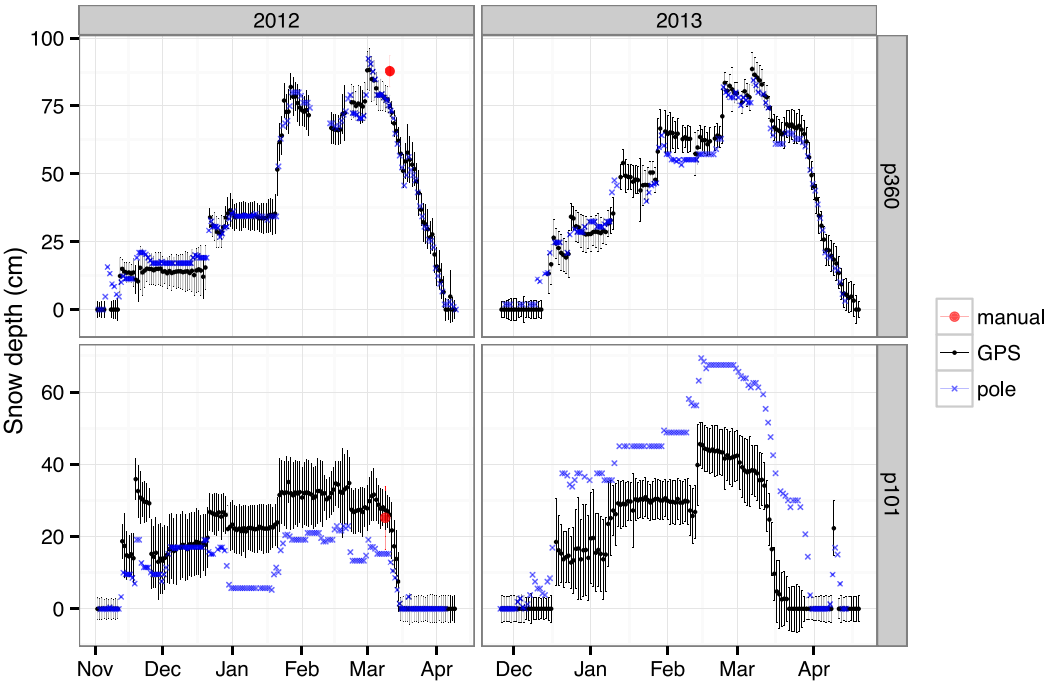

Figure 8. GPS (black), manual (red), and time-lapse snow pole (blue) snow depth measurements at P101 (bottom) and P360 (top). Manual observations were only made in 2012 at these sites. Error bars for GPS and manual measurements are the same as in Figure 7.

and in situ SWE are in closer agreement. The first manual observation in 2013 is the only one in the 2 years that lies beyond 1 standard deviation of the GPS-based estimate. The GPS-manual differences are much less during the remainder of 2013. The three instances of SWE underprediction demonstrate how even small depth errors can be magnified by the density model. In general, depth underestimation will result in bulk density that is too low, yielding an underestimation of SWE. The opposite occurs when depth is overestimated. Therefore, if GPS snow depth is biased, it is reasonable to expect similar bias in the modeled density and SWE products.

In Figure 8, we compare GPS snow depth time series to snow depth measured by time-lapse photography at two PBO sites (P360 and P101) during the 2012 and 2013 water years. At P360, GPS snow depth closely tracks the snow pole measurement throughout the season, including the timing of accumulation and melt. On the day of the manual validation measurement (March 2012), depth at the snow pole and the GPS-derived depth are equal and approximately 10 cm below the site-average snow depth. At P101, the fluctuations in depth associated with accumulation and melt are again similar between the GPS and time-lapse data, but there are substantial differences in magnitude. Differences between the GPS snow depth and the time-lapse measurement change sign between the 2012 and 2013 water years. This was likely caused by the relocation of the snow pole during the intervening summer. On the date of manual measurement (March 2012), GPS-derived depth was nearly identical to site-averaged depth (Table 1b and Figure 8), whereas depth at the snow pole was more than 10 cm lower. The large bias, both positive and negative, of a point measurement within the GPS footprint at P101 underscores the need for representative areal measurements to appropriately validate the GPS method. Comparison of these measurements highlights the utility of the large GPS sampling footprint, compared to data from other automated methods that sample at a scale of $\sim$1 m^2.

4. Discussion

4.1. Sources of Error in GPS-Based Depth and Density

The validation data demonstrate that snow depth, density, and SWE estimated at PBO H_2O GPS sites are accurate. At most sites, depth errors are less than 5 cm and SWE errors are less than 2 cm. Similarly, density errors in most cases are less than 0.02 g cm^{-3}, small compared to errors associated with measuring density

in snow pits. Some portion of the observed differences likely results from how the manual and GPS data represent an average of the ~1000 m^2 area around the antenna. For example, the manual depth transects do not coincide exactly with the GPS ground tracks (Figure 4), especially at sites with few usable tracks. We now discuss other possible sources of depth and density errors that are revealed by the validation data described above. Sources of SWE errors are not discussed separately, given the direct dependence of SWE on the other two variables.

A small negative bias is the most consistent feature of the GPS snow depth errors. The validation data show that GPS snow depth tends to be ~5 cm less than the average from manual observations. Excluding the four sites with less than four usable tracks, which undersample the GPS footprint, reduces the bias from −6 to −3 cm. This negative bias in the GPS depth estimates can be explained by two different factors, both of which may have affected our results. First, some portion of the received GPS signal is reflected from below the snow surface, either from within the snowpack or the underlying soil. These reflections will result in an underestimation of snow depth. This type of error is greatest when there is fresh, low-density snow at the surface, which reduces the permittivity contrast of the air-snow interface. Second, the bare ground surface used to estimate GPS snow depth may be several centimeters higher (relative to the antenna) than the ground surface sensed by the manual snow probe. The former is determined at each site based on reflection data from before and after the snow season. The manual probe may penetrate further into the vegetation litter and surface soil than this apparent reflection surface, yielding a negative bias in GPS snow depth.

Application of the *McCreight and Small* [2014] density model to PBO H_2O sites was successful. The negative bias in GPS snow depth observations was small enough so that effects on density estimates were negligible. In addition, estimation of model parameters using depth and density measurements from SNOTEL sites did not obviously degrade density errors relative to the estimated errors. On average, GPS sites are ~400 m lower than the SNOTEL sites within 70 km that are used to identify model. In addition, many SNOTEL sites tend to be in small clearings within forests whereas the GPS sites in PBO H_2O are situated in more exposed areas. Even with these physiographic differences, errors reported here were nearly identical to those calculated for application of the model to SNOTEL sites [*McCreight and Small*, 2014]. This suggests that the model parameters are robust at the ~100 km scale for applications at peak accumulation, even given significant differences in elevation and vegetation.

Though the density model is not a great source of error, examination of the largest density errors provides some insight into its application. Fourteen of 16 modeled density estimates were very accurate, together yielding an RMSE of 0.02 g cm^{-3}. The model overestimated density at P023 by 0.05 g cm^{-3}, an error similar in magnitude to errors associated with measuring density in snow pits. Therefore, it is difficult to learn anything conclusive about model performance from the overestimation at P023. In contrast, the error was much larger at P019 and warrants investigation. The modeled density was 0.33 g cm^{-3} and the observed density was 0.44 g cm^{-3}, which was the highest value observed at all of the sites. Two factors likely contributed to the model underestimation. First, it was raining at P019 while the in situ data were being collected. This rainfall event increased density by ~0.04 g cm^{-3} over a 2 day interval at a SNOTEL site ~5 km away and at similar elevation. The rainfall likely had a similar effect on density at P019. The model does not include rainfall as an input, and thus predicted density did not increase during this event. The second factor contributing to the error was that the snowpack was far below average in 2012. There had been little accumulation during the 2 months prior to the date of manual observation, which is very abnormal for this site. As a result, densification of the snowpack likely progressed more rapidly than in a typical year. Densities of 0.44 g cm^{-3}, observed in mid-March in 2012, do not appear in the density climatology of fit for P019 until mid-May, just before melt out.

4.2. Are the Validation Data Representative of Conditions in the PBO H_2O Network?

The accuracy of GPS-based depth, density, and SWE was established using data from 18 PBO H_2O sites. The results presented above only constrain the network-wide errors if the validation sites are representative of the ~130 snow sites throughout the network (Figure 1). The primary factor to consider when comparing the sites used for validation and snow sites in the network is the number of usable ground tracks. Our results show that the number of usable ground tracks affects the accuracy of site-averaged snow depth estimates, and therefore estimates of SWE. The number of usable tracks was considered when the validation sites were chosen. However, it was of secondary importance in site selection relative to issues associated

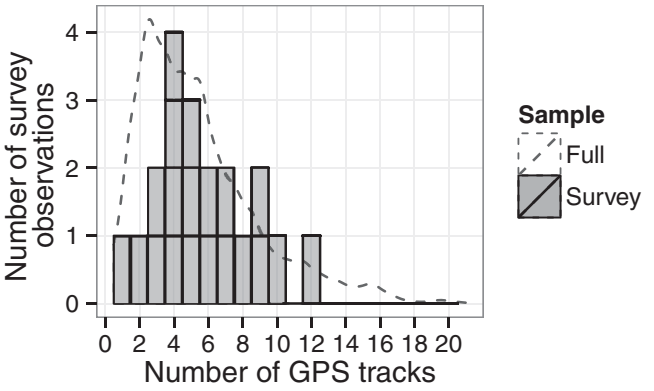

Figure 9. Distribution of the number of usable GPS ground tracks for snow depth estimates. The histogram and the *y* axis correspond to the validation sites. The dashed line shows the distribution of usable GPS tracks for all PBO H_2O depth measurements greater than 10 cm (13,303 measurements at 130 sites), which is not scaled to *y* axis (the mode is 3 GPS tracks with 2158 observations).

with site access and location relative to other validation sites. The distribution of usable ground tracks is similar between the subset of sites used for validation and the full network (Figure 9). Above, we showed that sites with four or more usable ground tracks tend to produce accurate snow depth estimates. GPS observations are based on four or more usable tracks 71% of the time in the PBO H_2O network and 80% of the time for the subset used for validation. Observations are based on five or more tracks with almost identical frequency (59%) in the two distributions.

Other factors need to be considered when evaluating if the errors estimated from the validation survey data are representative of PBO H_2O. We quantified GPS snow depth errors around the time of peak accumulation. Snow depth errors did not depend on the magnitude of the snow depth observations, so the peak-accumulation errors are likely representative of errors throughout the snow season. This is supported by time series comparison at RN86 (Figure 7).

In contrast, density errors should be smallest at peak accumulation. *McCreight and Small* [2014] showed that the density model errors were greatest at the beginning and end of the snow season, based on an analysis of SNOTEL data. However, this analysis applied to generally deep snowpacks of SNOTEL, which are quite different from those observed at many PBO H_2O locations. For snow depths greater than roughly 30 cm, density errors have a relatively limited effect on SWE errors: the density errors are nearly always less than 0.04 g cm^{-3} so SWE errors are dominated by snow depth errors. Density errors tend to be larger for snow depths less than approximately 30 cm [e.g., *McCreight and Small*, 2014]. Though such errors were not found (e.g., P088, P118, P460) in this study, density estimates for shallow snow are more uncertain. Density errors are likely greatest for very shallow snow ($<$10 cm) and will depend on snowpack temporal evolution. However, in these cases, SWE is very close to zero regardless of the density value used in the calculation. We estimate that the SWE errors reported here are representative of all PBO H_2O network observations for depths greater than 30 cm. The SWE errors may also be appropriate at snow depth above 10 cm for locations with low-variability seasonal evolution to date of observation, however, additional validation data would be useful to more completely describe SWE errors throughout the snow season.

Based on this comparison and the results presented above, we conclude the following about the accuracy of snow depth and SWE estimates at PBO H_2O sites. First, the validation data provide a representative description of errors at snow sites throughout the PBO H_2O network. Second, snow depth and SWE estimates are more reliable when many ground tracks are used at a site. Four or more usable tracks are available for 71% of PBO H_2O snow depth observations, which yield more accurate estimates. Snow depth estimated at sites with one to three usable tracks ($\sim$30% of PBO H_2O snow sites) may closely match the average depth across the $\sim$1000 m^2 footprint (e.g., P023 in Table 1b). However, there is no way to confirm that this is the case without continuous site visits. Thus, snow depth and SWE estimates from these sites should be considered to have more uncertainty. Users of daily GPS snow depth observations may choose to apply a bias correction. The bias may be slightly larger at sites with only several GPS tracks. However, the validation data set is insufficient to describe exactly how the bias varies with the number of ground tracks. Because the snow depth bias will have little effect on density estimates, the SWE bias correction should be calculated as the product of bias-corrected depth and the estimated density.

4.3. Considerations for Future Installations of GPS Antennas to Measure Snow Depth

With the exception of RN86, all the sites used in this study were installed to study tectonic plate boundary deformation, not for measuring snow depth. The selection of new sites for measuring snow depth using

reflected GPS signals should consider several constraints. GPS-based estimates of snow depth are most reliable when many ground tracks are used and spatial variability of snow depth is not extreme. The primary limitation on the number of satellite tracks used is the GPS constellation itself. PBO H_2O is currently based on using the L2C signal, which only began transmission for satellites launched after 2005 [*Larson and Nievinski*, 2013]. At the time that this study was conducted, only 9 L2C transmitting satellites were available. Since that time, four more satellites have been launched; two more satellites are scheduled to be launched in fall 2014. The end result is that the spatial coverage of the GPS method and the accuracy of the PBO H_2O retrievals is improving with time. Terrain and vegetation around the antenna also impact the number of ground tracks that yield usable data. Sites with extensive bedrock outcrops, slopes greater than $\sim 10^{\circ}$, or otherwise complex topography should be excluded. Tall vegetation obstructs the GPS signal, making some ground tracks unusable (see discussion and examples in *Larson and Nievinski* [2013]). For example, tracks to the northwest and east of RN86 are unusable due to trees (Figure 4). In most cases, problematic terrain and vegetation can be identified from digital elevation models (DEMs) and Google Earth images. Terrain and vegetation also affect the spatial variability of snow. Studies suggest that patterns of snow depth spatial variability are relatively stable on interannual time scales [e.g., *Deems et al*., 2008]. Therefore, it might be worthwhile to survey snow depth at candidate sites in the winter before GPS installation to quantify snow depth variability.

The infrastructure used at GPS sites in general (and PBO in particular) was not designed for sensing snow depth and could be improved for future installations. For example, many PBO antennas are installed approximately 2 m above the ground surface. Mounting antennas higher above the surface (e.g., at 3 m) would be beneficial for snow sensing in two ways. First, a higher antenna increases the size of the GPS measurement footprint. Second, a higher antenna would limit the instances when the antenna is not at least two wavelengths above the snow surface. Encroachment of snow on the antenna is rarely an issue at PBO H_2O sites. Less than 1.5% of the depth observations are within 0.6 m of the antenna height. However, antenna height is an important consideration for installations in areas of deeper snow. Manual data were collected at P351, but the snow surface was nearly at the antenna height, so GPS snow depth data available for comparison was known to be inaccurate. If the validation data had been collected in a normal snow year, data from several other sites may have been similarly affected. Raising the antenna in snowy regions would also benefit geophysicists—who currently must throw out all data when the antenna has been covered with snow. This has been a particular problem in Alaska, where many of the PBO sites were set at 1.5 m above bare soil and are regularly covered by snow each winter.

Antennas used by geodesists were designed to some extent to suppress reflections and thus are not optimal for sensing snow depth. These GPS systems are also relatively expensive (more than $5K per unit at the nonprofit, group purchase price). If the only purpose of the instrument was to measure snow depth, a cheaper instrument could be designed and deployed for snow sensing. However, given the costs of maintaining the instrumentation in any network and the cost of data telemetry, combining the geodetic networks with snow sensing has significant advantages.

4.4. Applications of GPS-Based Snow Products

GPS-based snow depth, density, and SWE from GPS sites can be used in a similar fashion to data streams from other snow observing networks. PBO H_2O snow products could be used to guide water resource management in snow-dominated watersheds. The near real-time GPS snow products, including error estimates, are updated daily (http://xenon.colorado.edu/portal). These allow the timing and rate of melt to be monitored with sufficient frequency for most applications. Another straightforward use of PBO H_2O snow data is to provide ground-truth of remotely sensed or modeled products. The relatively large sampling footprint of the GPS reflections data is advantageous in this application, compared to point or ~ 1 m^2 measurements.

PBO H_2O complements sites in the SNOTEL network. Sites in both networks are distributed throughout the western U.S. However, the PBO H_2O sites have very different physiographic conditions than most SNOTEL sites. First, SNOTEL sites are typically located in small clearings within forests and provide information about snowpack protected by forest canopies. In contrast, PBO H_2O sites are necessarily located in either very large clearings, adjacent to forested areas (Figures 2a and 2b), or in nonforested ecosystems (Figure 2c). Thus, the effects of vegetation on snow accumulation and melt are different at PBO H_2O and SNOTEL sites. Second, GPS snow sites are typically at lower elevations (440 m lower, on average) than neighboring

SNOTEL sites. The combined effects of lower elevation and less vegetation result in shallower snow at many PBO H_2O sites, compared to SNOTEL sites within the same region. Thus, the PBO H_2O snow products provide a novel set of data. These data may be useful for improving assimilated snow products (e.g., SNODAS) which may be biased in physiographic regions underrepresented by current observing networks [*Clow et al.*, 2012].

5. Conclusions

Snow products derived from GPS reflections data closely match snow depth, density, and SWE measured in situ at 18 PBO H_2O sites. The validation comparison was completed around the time of peak accumulation. Daily snow depth derived from GPS is very similar to mean snow depth measured within a 25 m radius of the antenna, or at the $\sim$1000 m^2 scale. There is a small negative bias (-6 cm) that is consistent across the range of snow depths measured, from no snow to 150 cm. The number of usable GPS ground tracks affects the error: when daily mean snow depth is computed using four or more tracks, the snow depth bias is only -3 cm. Modeled snow bulk density, based on GPS snow depth time series, closely matched density measured in a single snow pit at each validation site. In 12 of 16 cases, density errors were less than 0.02 g cm^{-3}. Combining GPS-based depth and density yields an accurate estimate of SWE over its observed range, from 0 to 60 cm ($R^2 = 0.97$ and bias $= -2$ cm). These results show that the near real-time PBO H_2O snow products have errors small enough for monitoring water resources in snow-dominated basins.

Acknowledgments

Data used in this paper are provided in Table 1 and are available online at: http://xenon.colorado.edu/portal/. This research was funded by NSF (EAR-0948957, AGS-0935725, EAR-1144221) and NASA (NNX12AK21G and NNH10ZDA001N). Some data, equipment, and engineering services were provided by the Plate Boundary Observatory operated by UNAVCO for EarthScope and supported by NSF (EAR-0350028 and EAR-0732947). We thank Jeffrey Buechler for collecting snow depth and density data. We thank Jobie Carlisle and the T.W. Daniels, Experimental Forest of Utah State University, for making in situ measurements at the RN86 site. We thank Jim Normandeau for coordinating the setup of the time-lapse cameras. Felipe Nievinski and Praveen Vikram helped with many technical issues. Kevin Sampson provided elevation data in Figure 1. The free and open-source R software [*R Development Core Team*, 2011] along with the reshape2, ggplot2, plyr, and scales packages [*Wickham*, 2007, 2009, 2011] were used for analysis and presentation.

References

Beniston, M. (2003), Climatic change in mountain regions: A review of possible impacts, in *Climate Variability and Change in High Elevation Regions: Past, Present & Future*, pp. 5–31, Springer, Netherlands.

Cayan, D. R. (1996), Interannual climate variability and snowpack in the western United States, *J. Clim.*, *9*(5), 928–948.

Clow, D. W., L. Nanus, K. L. Verdin, and J. Schmidt (2012), Evaluation of SNODAS snow depth and snow water equivalent estimates for the Colorado Rocky Mountains, USA, *Hydrological Processes*, *26*(17), pp. 2583–2591.

Cohen, J., and D. Entekhabi (1999), Eurasian snow cover variability and Northern Hemisphere climate predictability, *Geophys. Res. Lett.*, *26*(3), 345–348.

Deems, J. S., S. R. Fassnacht, and K. J. Elder (2008), Interannual consistency in fractal snow depth patterns at two Colorado mountain sites, *J. Hydrometeorol.*, *9*(5), 977–988.

Dickinson, W. T., and H. R. Whiteley (1972), A sampling scheme for shallow snowpacks, *Hydrol. Sci. Bull.*, *17*(3), 247–258.

Dietz, A. J., C. Kuenzer, U. Gessner, and S. Dech (2012), Remote sensing of snow—A review of available methods, *Int. J. Remote Sens.*, *33*(13), 4094–4134.

Dixon, D., and S. Boon (2012), Comparison of the SnowHydro snow sampler with existing snow tube designs, *Hydrol. Processes*, *26*, 2555–2562, doi:10.1002/hyp.9317.

Elder, K. J., J. Dozier, and J. Michaelsen (1991), Snow accumulation and distribution in an alpine watershed, *Water Resour. Res.*, *27*(7), 1541–1552.

Farnes, P. E., N. R. Peterson, B. E. Goodison, and R. P. Richards (1982), Metrication of Manual Snow Sampling Equipment 705-82, in *Proceedings of the Western Snow Conference*, vol. 30, p. 437, Colorado State University.

Garvelmann, J., S. Pohl, and M. Weiler (2013), From observation to the quantification of snow processes with a time-lapse camera network, *Hydrol. Earth Syst. Sci.*, *17*, 1415–1429, doi:10.5194/hess-17–1415-2013.

Goodison, B. E., J. E. Glynn, K. D. Harvey, and J. E. Slater (1987), Snow surveying in Canada: A perspective, *Can. Water Resour. J.*, *12*(2), 27–42.

Gutmann, E. D., K. M. Larson, M. W. Williams, F. G. Nievinski, and V. Zavorotny (2012), Snow measurement by GPS interferometric reflectometry: An evaluation at Niwot Ridge, Colorado, *Hydrol. Processes*, *26*(19), 2951–2961.

Harpold, A. A., et al. (2014), A LiDAR derived snowpack dataset from mixed conifer forests in the Western U.S., *Water Resour. Res.*, *50*, 2749–2755, doi:10.1002/2013WR013935.

Johnson, J. B., A. Gelvin, and G. Schaefer (2007), An engineering design study of electronic snow water equivalent sensor performance, in *75th Annual Western Snow Conference*, pp. 16–19. [Available at http://www.westernsnowconference.org/node/704.]

Jonas, T., C. Marty, and J. Magnusson (2009), Estimating the snow water equivalent from snow depth measurements in the Swiss Alps, *J. Hydrology*, *378*(1), pp. 161–167.

Larson, K. M., and F. G. Nievinski (2013), GPS snow sensing: Results from the EarthScope Plate Boundary Observatory, *GPS Solutions*, *17*(1), 41–52.

Larson, K. M., E. D. Gutmann, V. U. Zavorotny, J. J. Braun, M. W. Williams, and F. G. Nievinski (2009), Can we measure snow depth with GPS receivers?, *Geophys. Res. Lett.*, *36*, L17502, doi:10.1029/2009GL039430.

Marchand, W., and A. Killingtveit (2004), Statistical properties of spatial snowcover in mountainous catchments in Norway, *Nord. Hydrol.*, *35*(2), 101–117.

McCreight, J. L., and E. E. Small (2014), Modeling bulk density and snow water equivalent using daily snow depth observations, *Cryosphere Discuss.*, *7*, 5007–5049. [Available at http://www.the-cryosphere-discuss.net/7/5007/2013/tcd-7-5007-2013.html.]

Nievinski, F. G., and K. M. Larson (2014a), Forward and inverse modeling of GPS multipath for snow depth estimation, I: Formulation and simulations, *IEEE Trans. Geosci. Remote Sens.*, *52*(10), 6555–6563, doi:10.1109/TGRS.2013.2297681.

Nievinski, F. G., and K. M. Larson (2014b), Forward and inverse modeling of GPS multipath for snow depth estimation, II: Application and validation, *IEEE Trans. Geosci. Remote Sens.*, *52*, 6564–6573, doi:10.1109/TGRS.2013.2297688.

Painter, T. H., K. Rittger, C. McKenzie, P. Slaughter, R. E. Davis, and J. Dozier (2009), Retrieval of subpixel snow covered area, grain size, and albedo from MODIS, *Remote Sens. Environ.*, *113*(4), 868–879.

Pomeroy, J. W., and D. M. Gray (1995), Snow accumulation, relocation and management, *NHRI Sci. Rep. 7*, 144 pp., Supply and Serv. Can., Saskatoon, Sask.
Press, F., S. Teukolsky, W. Vetterling, and B. Flannery (1996), *Numerical Recipes in Fortran 90: The Art of Parallel Scientific Computing*, 2nd ed., Cambridge Univ. Press, Cambridge, U. K.
R Core Team (2014), *R: A Language and Environment for Statistical Computing. R Found*. For Stat. Comput., Vienna, Austria.
Rittger, K., T. H. Painter, and J. Dozier (2013), Assessment of methods for mapping snow cover from MODIS, *Adv. Water Resour.*, *51*, 367–380.
Ryan, W. A., N. J. Doesken, and S. R. Fassnacht (2008), Evaluation of ultrasonic snow depth sensors for US snow measurements, *J. Atmos. Oceanic Technol.*, *25*(5), 667–684.
Serreze, M. C., M. P. Clark, R. L. Armstrong, D. A. McGinnis, and R. S. Pulwarty (1999), Characteristics of the western United States snowpack from snowpack telemetry (SNOTEL) data, *Water Resour. Res.*, *35*(7), 2145–2160.
Stepphun, H., and G. E. Dyck (1974), Estimating the true basin snowcover, in *Advances Concepts and Techniques in the Study of Snow and Ice Resources, Asilomar Conference Grounds, Monterey, CA, USA*, Natl. Acad. Of Sci., Washington, D. C.
Sturm, M. (2009), Field techniques for snow observations on sea ice, in *Field Techniques for Sea-Ice Research*, edited by H. Eicken et al., pp. 25–48, Univ. of Alaska Press, Fairbanks.
Sturm, M., B. Taras, G. Liston, C. Derksen, T. Jonas, and J. Lea (2010), Estimating snow water equivalent using snow depth data and climate classes, *J. Hydrometeorol.*, *11*(6), 1380–1394.
Walsh, J. E. (1984), Snow cover and atmospheric variability: Changes in the snow covering the earth's surface affect both daily weather and long-term climate, *Am. Sci.*, *72*(1), 50–57.
Wickham, H. (2007), Reshaping data with the reshape package, *J. Stat. Software*, *21*(12), 1–20.
Wickham, H. (2009), *ggplot2: Elegant Graphics for Data Analysis*, Springer.
Wickham, H. (2011), The split-apply-combine strategy for data analysis, *J. Stat. Software*, *40*(1), 1–29.